Nano Energy 47 (2018) 294–300

Contents lists available at ScienceDirect

Nano Energy

journal homepage: www.elsevier.com/locate/nanoen

Full paper

# Pseudocapacitive layered iron vanadate nanosheets cathode for ultrahigh-rate lithium ion storage

Qiulong Wei[a,1], Qinqin Wang[c,1], Qidong Li[a], Qinyou An[a,**], Yunlong Zhao[d], Zhuo Peng[a], Yalong Jiang[a], Shuangshuang Tan[a], Mengyu Yan[a], Liqiang Mai[a,b,*]

[a] State Key Laboratory of Advanced Technology for Materials Synthesis and Processing, International School of Materials Science and Engineering, Wuhan University of Technology, Wuhan 430070, PR China
[b] Department of Chemistry, University of California, Berkeley, CA 94720, USA
[c] Institute of Physics, Chinese Academy of Sciences, Beijing 100190, PR China
[d] Department of Chemistry and Chemical Biology and Harvard John A. Paulson School of Engineering and Applied Sciences, Harvard University, Cambridge, MA 02138, USA

ARTICLE INFO

*Keywords:*
Two-dimensional materials
Pseudocapacitive cathode
Layered iron vanadate
Lithium storage
High rate

ABSTRACT

Pseudocapacitive charge storage has been regarded as a promising mechanism to achieve both high specific energy and power energy storage devices. Some pseudocapacitive anode materials show great high-rate performance, however, it remains a significant challenge to develop the cathode ones. Herein, for the first time, we report a layered iron vanadate ($Fe_5V_{15}O_{39}(OH)_9{\cdot}9H_2O$, named as kazakhstanite) nanosheets (FeVO NSs) with featuring ultrathin layer thickness (< 10 nm). The FeVO NSs are synthesized by a facile wet-chemical approach with a high yield. Compared to the FeVO nanoparticles, the crystalline layered FeVO NSs have additional interlayered $Li^+$ storage sites, leading to the enhanced capacity. *Ex-situ* X-ray diffraction results demonstrate a non-phase change process and there is only ~ 1.1% layer expansion/shrinkage during lithiation and delithiation process. Based on detail kinetics analysis and *ex-situ* X-ray photoelectron spectroscopy results, it is found that over 70% of total capacity is pseudocapacitive contribution, which contributes to the ultrahigh-rate capability (a high capacity of 350, 273 and 90 mAh $g^{-1}$ is achieved at 0.1, 1 and 20 A $g^{-1}$, respectively) and excellent cycling stability over thousands of cycles. This work presents the high performance vanadate material that delivers highly pseudocapacitive behavior, and provides a promising direction to realize both high energy and high power lithium storage.

## 1. Introduction

Rechargeable lithium ion batteries (LIBs) have been widely used in our daily life, including mobile electronics, electric vehicles and renewable energy storage [1–3]. Conventional LIB cathode material provides the $Li^+$ intercalation channels and host sites [4,5]. Their charge storage kinetics is mainly determined by the $Li^+$ diffusion within the structure: $Li^+$ firstly intercalate into the structure and then diffuse to an accessible redox site. The slow diffusion process requires prolonged charging time and limits the rate capability [6–8]. Pseudocapacitance, as another intensively-studied charge storage system, exhibits similar faradaic redox reactions but with much faster diffusion kinetics, which yields great potential for achieving high energy density at fast charge and discharge rates [2,4–10]. Most recently, the concept of intercalation pseudocapacitance, proposed by Dunn and co-workers, shows the advantages that not only the surface but also the whole bulk of materials are utilized, enabling higher energy density accompanied with high power [3–7]. This intercalation pseudocapacitance were mostly observed in layered materials which enable fast $Li^+$ diffusion between the layers without significant structural changes [7,8,10–13]. Further work demonstrated that the nanosized morphology with shortened diffusion distances enhanced the electrochemical performances [8]. Up to date, most of the reported fast $Li^+$ ion pseudocapacitive materials were anodes (*T*-$Nb_2O_5$, [7,10] $TiO_2$, [11] $MoS_2$, [12] and $TiS_2$ [13]). Further search of pseudocapacitive cathode materials with higher capacity above 300 mAh $g^{-1}$ and fast charge/discharge rates is

* Corresponding author at: State Key Laboratory of Advanced Technology for Materials Synthesis and Processing, International School of Materials Science and Engineering, Wuhan University of Technology, Wuhan 430070, PR China.
** Corresponding author.
*E-mail addresses:* anqinyou86@whut.edu.cn (Q. An), mlq518@whut.edu.cn (L. Mai).
[1] These authors contributed equally to this work.

https://doi.org/10.1016/j.nanoen.2018.02.028
Received 10 September 2017; Received in revised form 23 January 2018; Accepted 12 February 2018
Available online 14 February 2018

significant but remains largely unexploited.

Layered orthorhombic vanadium pentoxide (α-$V_2O_5$) owns a high reversible capacity of 294 mAh $g^{-1}$ (with two $Li^+$ intercalation per formula), which is much higher than that of the $LiCoO_2$, $LiMn_2O_4$ and $LiMO_2$ (M = Co, Mn, Ni or Al mixed compounds) [14–17]. Meanwhile, the abundance of vanadium sources make it as very attractive candidates for energy storage applications. However, the sluggish $Li^+$ ion diffusion, poor electron conductivity, and irreversible phase transitions upon deep cycling result in poor rate capability and cyclability, which pose the challenges to further applications [16]. Searching from the crystallology, it is found that lots of vanadates are layered materials which provide the diffusion channels for $Li^+$ storage [18,19]. Recently, some researches on the vanadates, such as alkali metal vanadates [20], silver vanadates (e.g. $Ag_2V_4O_{11}$) [19] and copper vanadates (e.g. $CuV_2O_6$) [21], metahewettite ($CaV_6O_{16}{\cdot}3H_2O$)[22] showed increased electronic conductivity, enlarged and stabilized layer structure without blocking the ions diffusion channels, which synergistically improved the electrochemical performances for lithium storage. As known, the iron vanadates are the most nature existence and abundant [18,23], such as Fervanite ($Fe_4V_4O_{16}{\cdot}5H_2O$), Navajoite ($FeV_9O_{24}{\cdot}12H_2O$), Kazakhstanite ($Fe_5V_{15}O_{39}(OH)_9{\cdot}9H_2O$) and so forth. The $Fe_5V_{15}O_{39}(OH)_9{\cdot}9H_2O$ has a large layered spacing ($d_{002}$ = 10.51 Å), which is very beneficial to the $Li^+$ storage. However, there are rarely reported upon this material used as LIB cathode and the detailed charge storage mechanism are unclear yet.

In this work, for the first time, we demonstrate the pseudocapacitive lithium storage behavior in the hydrated layered iron vanadate (kazakhstanite $Fe_5V_{15}O_{39}(OH)_9{\cdot}9H_2O$, noted as FeVO). The crystalline FeVO with an ultrathin nanosheet (NS) morphology is prepared by a facile artificial synthesis approach with high yield. Compared to the electrochemical performance of amorphous FeVO nanoparticles (NPs), the crystalline layered FeVO NSs cathode delivers much enhanced capacity, rete capability and cycling stability. The *ex-situ* X-ray diffraction (XRD) results indicates a non-phase charge process for the FeVO NSs during repeated lithiation/delithiation. Detailed kinetics analysis and *ex-situ* X-ray photoelectron spectroscopy (XPS) results confirm that the pseudocapacitive behavior dominates the charge storages, which is beneficial to achieve ultrahigh-rate capability. The presented pseudocapacitive cathode (layered FeVO NSs) with excellent electrochemical performance exhibits the great practical potentials for further achieving both high-capacity and high-rate energy storage devices.

## 2. Experimental section

### 2.1. Experimental methods

#### 2.1.1. Synthesis of hydrated iron vanadate nanosheets and nanoparticles

The activated material was synthesized by a facile water bath method. Typically, $NH_4VO_3$ (3 mmol) was added in de-ionized water (100 mL) under magnetic stirring at 90 °C until its total dissolution. Then $Fe(NO_3)_3$ $9H_2O$ solution (0.1 M, 10 mL) was slowly dropped into $NH_4VO_3$ solution under continuous stirring and kept at 90 °C for another one hour. Then the brown precipitates were collected by centrifugation and washed with de-ionized water three times and pure ethanol for another three times. After washing, the products (FeVO NSs) were dried in vacuum oven at 80 °C for 12 h. The amorphous FeVO nanoparticles were obtained from the precipitates with only one minute water bath reaction.

### 2.2. Materials characterization

X-ray diffraction (XRD) measurements were performed using a D8 Advance X-ray diffractometer with a non-monochromated Cu Kα X-ray source. Scanning electron microscopy (SEM) images were collected by using a JEOL-7100F microscope. Transmission electron microscopy (TEM) and high-resolution TEM (HRTEM) images were collected by using a JEM-2100F STEM/EDS microscope. Fourier transform infrared (FT-IR) transmittance spectra were recorded using the 60-SXB IR spectrometer. Brunauer-Emmett-Teller (BET) surface area was measured by using Tristar II 3020 instrument. Thermogravimetric (TG) analysis was performed using NETZSCH-STA449c/3/G thermoanalyzer. Inductively coupled plasma (ICP) test was performed on the PerkinElmer Optima 4300DV spectrometer. X-ray photoelectron spectroscopy (XPS) was recorded with a VG Multilab 2000.

### 2.3. Electrochemical measurements

Standard CR2025-type coin cells were assembled in an Ar-filled glove box. The working electrodes were prepared by mixing 70% active material, 20% ketjen black and 10% carboxyl methyl cellulose (CMC) binder, and then coated on a carbon coated Al (C@Al) foil. After drying in vacuum oven at 120 °C for 6 h, the electrodes were punched into 10 mm diameter with an active material mass loading of 1–6 mg $cm^{-2}$. For lithium storage test, lithium foil was used as the anode and 1 M $LiClO_4$ in propylene carbonate (PC) was used as the electrolyte. Galvanostatic charge/discharge and cyclic voltammetrys (CV) were performed by using Bio-Logic VMP3 potentiostats at room temperature. For ex-situ XRD tests the electrode was sealed by tape and for directly texts.

## 3. Results and discussion

The FeVO compound was prepared by a facile co-precipitation and a crystal growth process under water bath (Fig. S1). At the beginning, precipitates formed directly after the mixing of iron nitrate and ammonium metavanadate solution. The incipient precipitates are nanoparticles with an average size of ~30 nm, as shown in SEM image (Fig. 1a). Then, the FeVO NPs orientated grew into crystalized NSs during sustained reaction (Fig. S1b-f). The as-formed thin nanosheets turned into oval microflowers to further reduce the surface energy. The FeVO NSs were obtained in high yield (Fig. S2). The TEM image further confirms the assembled nanosheets morphology (Fig. 1c). The HRTEM image (Fig. 1d) of the nanosheet edge shows the layered fringe indicating a lattice spacing of 1.0 nm. The thickness of the nanosheet is below 10 nm, which implies that the nanosheet composed of several atomic layers.

Fig. 1e shows the powder XRD patterns of the as-synthesized products. The FeVO NPs are amorphous state. Conversely, the FeVO NSs exhibit the crystalline diffraction peaks. All the peaks can be indexed to a pure phase of $Fe_5V_{15}O_{39}(OH)_9$ $9H_2O$ (JCPDS Card No. 46–1334, monoclinic, $a$ = 11.84 Å, $b$ = 3.65 Å, $c$ = 21.27 Å, $\beta$ = 100°), an iron-vanadium mineral named as kazakhstanite [23]. Additionally, the inductively coupled plasma (ICP) analysis (Table S1) figures out the atomic ratio of V: Fe is 3.013:1, very close to the stoichiometric ratio. The large $d_{002}$ = 10.6 Å is closed to the HRTEM observation (Fig. 1d), while the slightly decreased layer spacing may be due to a partial dehydration process under the electron beam. The HRTEM image (Fig. S3) of a NS reveals the inner-layer information. The lattice spacing of 3.56 and 2.71 Å corresponds to (204) and (− 115) planes, respectively, which is consistent with the XRD results. The energy dispersive X-ray spectroscopy (EDS) mapping (Fig. S2b) shows the uniform distribution of Fe, V and O in the NSs. The BET surface area of NSs and NPs is 34 and 40 $m^2$ $g^{-1}$, respectively.

The samples were further characterized by FT-IR (Fig. 1f). For the NPs, only peak at 801 $cm^{-1}$ (V–O–V vibrations) was observed owing to its amorphous state. For the layered NSs, the peaks at 537 $cm^{-1}$ (out-of-plane V-O-V vibrations) and 1004 $cm^{-1}$ (V=O stretching bond) occurs, which is characteristic for vanadium oxide layered structure [24]. The peak at 1400 $cm^{-1}$ indicates the existence of $NH^{4+}$, which comes from the added ammonium metavanadate [17]. The peak around 3400 $cm^{-1}$ is assigned to the stretching vibration of O–H band [24]. The symmetric band at 1624 $cm^{-1}$ comes from the δ($H_2O$) vibrations, which indicates

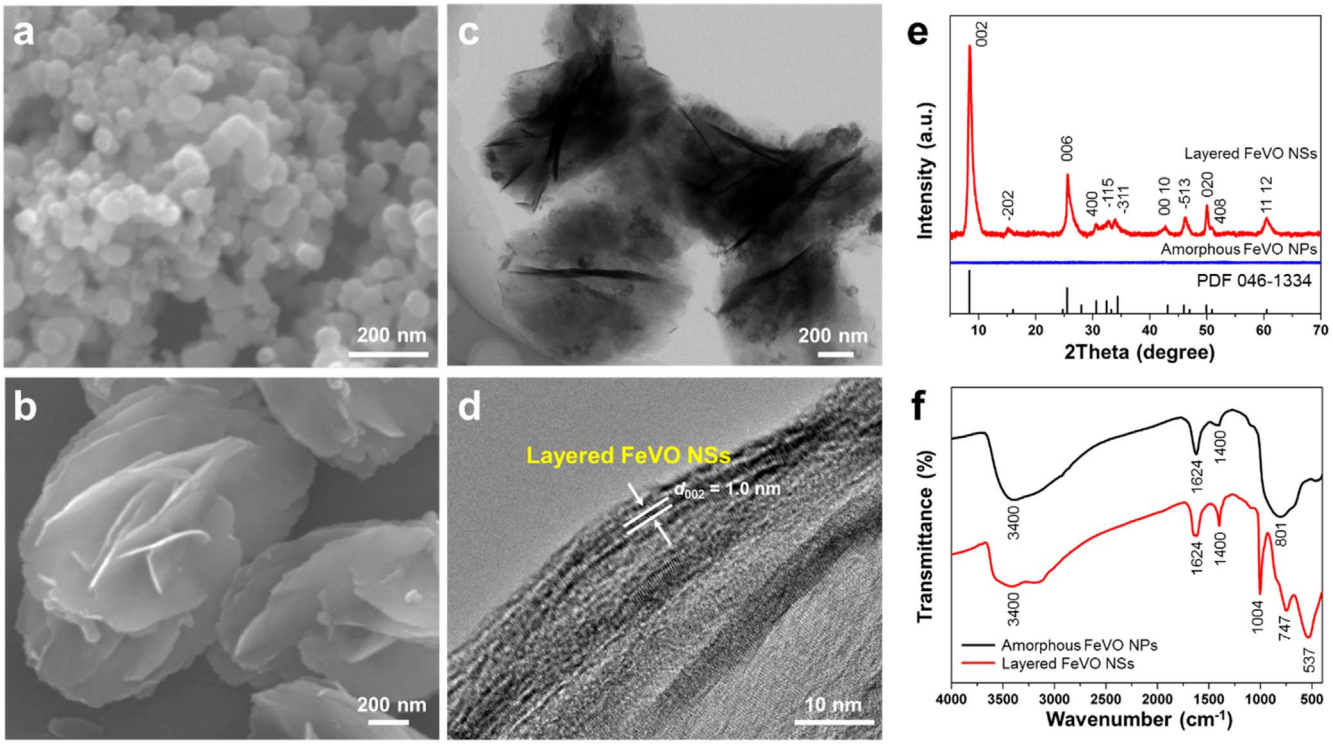


**Fig. 1. Morphology and phase characterization.** SEM images of amorphous FeVO NPs (a) and layered FeVO NSs (b), respectively. TEM image (c) and HRTEM image (d) of layered FeVO NSs. XRD patterns (e) and FTIR spectra (f) of the amorphous FeVO NPs and layered FeVO NSs, respectively.

the existence of water molecules. TG analysis was further to investigate the water contents. The TG curve of the FeVO NSs sample (Fig. S4) shows the multi-step mass losses, indicating the existence of different types of water in the material. The total content of weight loss is ~17%, which is slightly higher than the theoretical water loss of $Fe_5V_{15}O_{39}(OH)_9 \cdot 9H_2O$ (~ 15.9%), owing to the high surface area of nanomaterials with more absorbed water [23].

Electrochemical performance was tested by assembling coin cells (type-2025) with metallic lithium as anode. Cyclic voltammetry (CV) measurements were firstly made at a scan rate of 0.5 mV $s^{-1}$ in the potential window of 1.5–4 V (vs. $Li^+$/Li). The CV curve of amorphous NPs cathode (Fig. 2a) shows a nearly rectangular shape over a broad potential range, which arises from the disorder nature of their amorphous structure. In contrast, the layered NSs cathode displays a rectangular box and a couple of well-defined redox peaks [13]. A cathodic peak at 2.53 V ($Li^+$ intercalation) and an anodic peak at 2.72 V ($Li^+$ extraction) are observed. The area of CV curve for FeVO NSs cathode is larger than that for the amorphous NPs one, indicating the FeVO NSs cathode delivers higher capacity. Comparing CV shapes, it is observed that the enhanced capacity for NSs almost comes from the redox peaks. The CV curves between the NSs and NPs are visually distinguishable, and the detail mechanism is worth investigating.

*Ex-situ* XRD of the electrodes at different discharge/charge states were further characterized. First of all, the XRD pattern of the pristine layered FeVO NSs cathode shows that the (002) diffraction was not changed after the electrode preparing process (Fig. S5). Figs. 2b and 2c exhibit the *ex-situ* XRD patterns and $d_{200}$ value variation at different charge/discharge states, respectively. Compared to the pristine sample, the (002) diffraction peaks shift to higher angles, which is attributed to the activation process that the intercalation of $Li^+$ ion enhances the coordination reaction with the stacked layer and reduces interlayer spacing distance.[15,24] During the lithiation and de-lithiation processes (from state i to ix), the (002) diffraction peaks shift slightly, indicating non-phase changes (a typical pseudocapacitive behavior) [4]. The $d_{002}$ values at each state are calculated and displayed in Fig. 2d. During the discharge and charge process, the layered lattice breathing (variation of $d_{002}$) is highly reversible. After the activation [25], the largest shrinkage of $d_{002}$ during the lithiation/de-lithiation processes is only ~0.1 Å, corresponding to ~1.1% layer expansion/shrinkage. The slight lattice breathing is beneficial for delivering

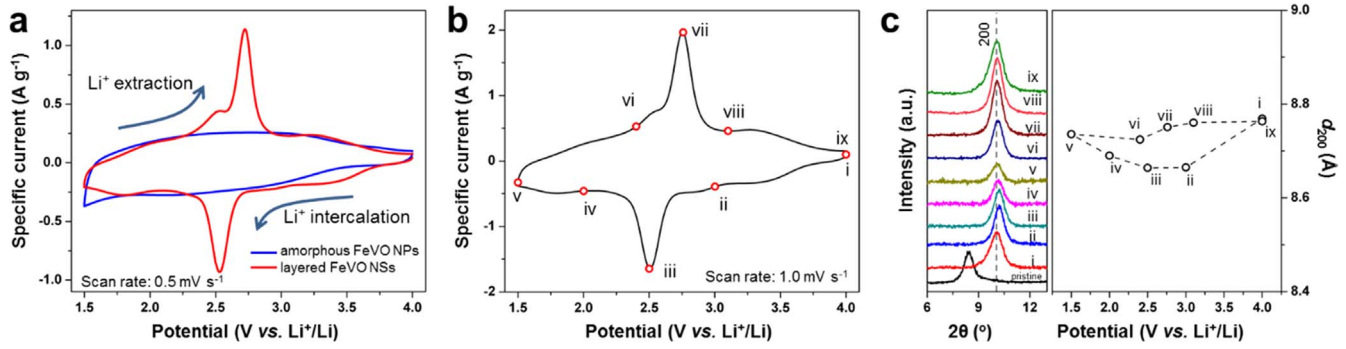


**Fig. 2. Lithium storage mechanism in layered FeVO NSs.** (a) CV curves of the amorphous NPs and layered NSs at a scan rate of 0.5 mV $s^{-1}$. CV curves for layered NSs at 1.0 mV $s^{-1}$ (b) and related *ex-situ* XRD patterns and $d_{200}$ value variation (c), respectively.

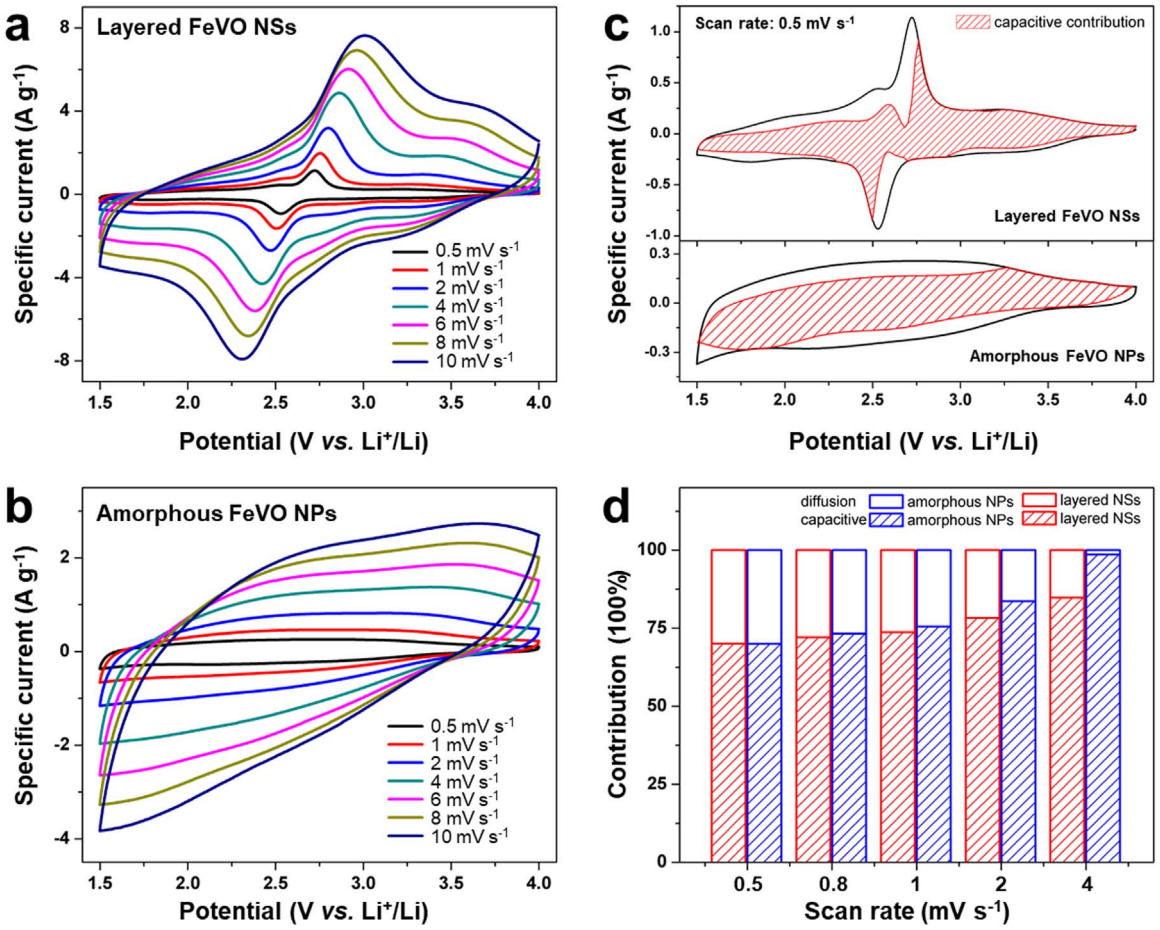


**Fig. 3. Kinetics analysis of layered NSs and amorphous NPs for lithium storage.** CV curves of layered NSs (a) and amorphous NPs (b) at various scan rates, respectively. Capacitive contributions (shaded area) to charge storage at a scan rate of 0.5 mV $s^{-1}$ (c) and normalized contribution ratio of capacitive and diffusion-controlled capacities at different scan rates (d) for layered NSs and amorphous NPs, respectively.

excellent cycling stability [26,27].

A kinetics analysis was further undertaken to supplementary understand the lithium storage behavior. CV curves measured at various scan rates (from 0.5 to 10 mV $s^{-1}$) are shown in Fig. 3a and b. The CV curves of the NSs (Fig. 3a) display the redox peaks with slight shifts with increasing scan rates, indicating excellent reaction kinetics. The CV curves of NPs (Fig. 3b) show the rectangular shape with the increasing scan rates. The twisted rectangular shape at fast scan rate may be due to the poor electronic nature of amorphous materials [8]. As proposed by Dunn and co-workers, it is further possible to distinguish the diffusion and the capacitive contribution occurs in the CV curves by using a detailed analysis [2,4]. The measured current ($i$) at a fixed potential (V) can be separated into capacitive effects ($k_1\nu$) and diffusion-controlled contributions ($k_2\nu^{1/2}$) (Eq. (1)), which is able to quantitatively characterize the capacity contribution of each part [4,28,29].

$$i(\mathrm{V}) = k_1\nu + k_2\nu^{1/2} \quad (1)$$

Fig. 3c shows the capacitive contribution of the both two samples (the shaded region). For the amorphous NPs, most of the capacity comes from the capacitive contribution, approaching to 70% of the total capacity even at the low scan rate of 0.5 mV $s^{-1}$. For the layered NSs, a large amount of the capacitive contribution (~70%) is still observed. A bulky electrolyte ($TBA^+$) was used to determine capacitive charge storage coming from faradaic redox or double-layer charge storage [8]. The radius of $TBA^+$ is quite large (~9 nm), which usually is unable to intercalate into the crystal structure, and the delivered capacity are electric double layer capacitance [8]. As shown in Fig. S6, for the $TBA^+$ electrolyte, no redox peaks are observed and much smaller capacity is obtained, indicating the capacitive contribution largely dependents on the pseudocapacitive lithium storage rather than the double-layer capacitance. Furthermore, *ex-situ* XPS spectra of V and Fe, and $^{57}$Fe Mössbauer spectra at pristine state, discharged state (Fig. 2b, state v) and charged state (Fig. 2b, state ix) were collected to supplementally prove the redox behavior of FeVO NSs (Fig. S7 and Table S2). It is found that the valence of vanadium and iron is reduced during discharge process and reversibly re-oxidized at the charged state, confirming the faradaic pseudocapacitive charge storage process and both V and Fe are electrochemical active. From the integration of fitting peaks, the contributed capacity from vanadium is much higher than that of iron.

Fig. 3c shows the divisive regions of the CV curves, the diffusion controlled regions are located predominantly around the redox peaks, which are expected to be diffusion limited. The extra redox peaks only occur in the crystalline FeVO sample (Fig. 2a), indicting the diffusion of $Li^+$ ions into its layered sites that delivers higher capacity. With the scan rate increasing, the percentage of capacitive contribution is promoted (Fig. 3d), owing to that the pseudocapacitance is advantaged for delivering high-rate capacity [7]. At the scan rate up to 4 mV $s^{-1}$, the capacitive contribution for the NSs and NPs increases to 84.8% and 98.6%, respectively. The systematical kinetics analysis demonstrates that the pseudocapacitive charge storage allows the layered FeVO NSs cathode delivering the excellent high-rate capacity.

Galvanostatic charge and discharge were subsequently measured to evaluate the electrochemical performance. Fig. 4a shows the charge-discharge curves of the layered NSs and the amorphous NPs at a specific current of 0.1 A $g^{-1}$. The amorphous FeVO NPs cathode displays slope

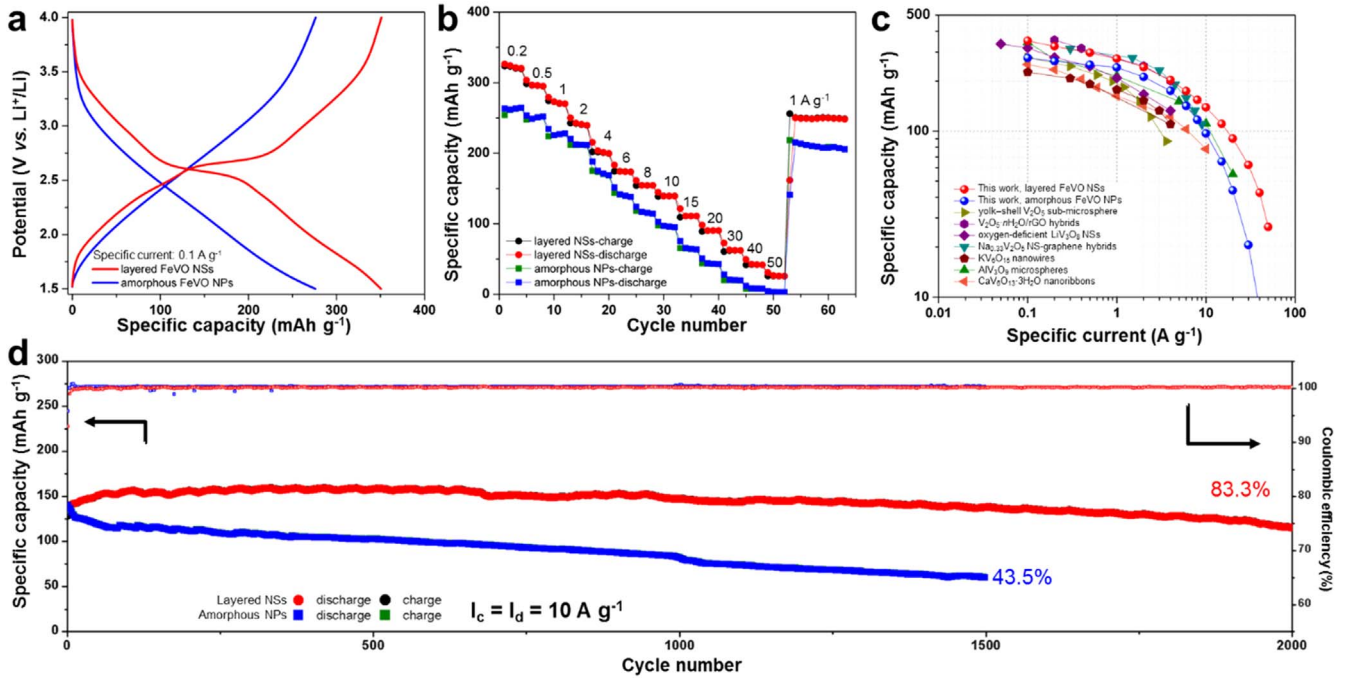


**Fig. 4. Galvanostatic performance of layered FeVO NSs and amorphous FeVO NPs for lithium storage.** (a) Galvanostatic charge – discharge curves of layered NSs and amorphous NPs at a specific current of 0.1 A $g^{-1}$. (b) Rate performance at various specific currents from 0.2 to 50 A $g^{-1}$. (c) Comparison of lithium storage rate performance of layered FeVO NSs to the state-of-the-art reported vanadium oxides and vanadates cathodes, yolk–shell $V_2O_5$ sub-microsphere [30], $V_2O_5{\cdot}nH_2O$/rGO hybrids [15], oxygen-deficient $LiV_3O_8$ NSs [31], $Na_{0.33}V_2O_5$ NS-graphene hybrids [32], $KV_6O_{15}$ nanowires [20], $AlV_3O_9$ microspheres [33], $CaV_6O_{13}{\cdot}3H_2O$ nanoribbons [22]. (d) Long-term cycling performances of layered NSs and amorphous NPs at a specific current of 10 A $g^{-1}$.

line curves, without any plateaus. However, the layered FeVO NSs cathode shows the slope lines and with the plateaus at ~ 2.6 V, consistent with the CV curves (Fig. 2a). The layered FeVO NSs deliver a capacity of 350 mAh $g^{-1}$, according to ~26 mol $Li^+$ per unit formula storage. The calculation is based on the equation: $n = (3.6MC)/F$, where $n$ represents the inserted ion amount (mol), $F$ represents the Faraday constant (C $mol^{-1}$), $C$ represents the capacity (mAh $g^{-1}$), and $M$ represents the molecular weight (g $mol^{-1}$). The capacity of FeVO NSs is much higher than that of NPs (275 mAh $g^{-1}$), while the enlarged capacity (~ 75 mAh $g^{-1}$) for NSs comes from the redox plateaus. Notice that the capacitive contribution is related to the surface area and crystal structure [3]. But the surface area of the layered FeVO NSs (34 $m^2$ $g^{-1}$) is slight low than that of amorphous FeVO NPs (40 $m^2$ $g^{-1}$). Therefore, the result of the enhanced capacity is due to the fact that $Li^+$ stores in the interlayers of crystalline FeVO NSs [10]. According to the electrochemical performance, *ex-situ* characterizations and kinetics analysis, the lithium ion storage mechanism of FeVO NSs is descripted as Eq. (2).

$$Fe_5V_{15}O_{39}(OH)_9{\cdot}9H_2O + xLi^+ + xe^- \leftrightarrow Li_xFe_5V_{15}O_{39}(OH)_9{\cdot}9H_2O (x< 26) \quad (2)$$

Rate capability of active material is a key factor for high-power application. Next, to investigate the rate capability, the FeVO cathodes were discharged and charged at progressively increased specific currents (ranging from 0.2 to 50 A $g^{-1}$), as shown in Fig. 4b. The NSs cathode delivers higher capacities than those of NPs at each current. The NSs cathode exhibits the capacities of 273, 242, 203 and 154 mAh $g^{-1}$ at 1, 2, 4 and 8 A $g^{-1}$, respectively. At higher current of 10, 20 and 50 A $g^{-1}$, a high capacity of 140, 90 and 27 mAh $g^{-1}$ is achieved, according to a charge/discharge time only ~ 50, 16 and 2 s, respectively. A comparison of the rate capabilities between our layered NSs and the state-of-the-art vanadium oxides and vanadates cathodes reported in the literatures is displayed in Fig. 4c [15,22,30–33]. The present layered FeVO NSs cathode delivers the remarkable high-rate capacity compared to the best reported results. Long-term cycling performance at a high specific current of 10 A $g^{-1}$ was tested as well (Fig. 4d). The amorphous FeVO NPs cathode just exhibits a capacity of 60 mAh $g^{-1}$ after 1500 cycles, corresponding to a capacity retention of 43.5%. But, the layered FeVO NSs still deliver a high capacity of 115 mAh $g^{-1}$ after 2000 cycles, corresponding to a capacity retention of 83.3%, which demonstrates the excellent pseudocapacitive charge storage processes in the crystalline layered structure.

Since it is the first time to report the FeVO as cathode for lithium storage, the calculation the power and energy density based on the mass of cathode material at various rates are calculated. Ragone plots of layered FeVO NSs and amorphous FeVO NPs cathodes are shown in Fig. S8 [34,35]. At the specific current of 0.1 A $g^{-1}$, it is found that the layered FeVO NSs cathode delivers an outstanding specific energy of 860 Wh $kg^{-1}$ at 246 W $kg^{-1}$, which is much higher than that of the amorphous NPs (630 Wh $kg^{-1}$ at 229 W $kg^{-1}$). The much enlarged energy density is due to the higher capacity and extra redox plateaus of layered FeVO NSs. Remarkably, for the layered NSs, a specific energy of ~ 400, 307 and 120 Wh $kg^{-1}$ at the specific average power of 13.8, 22.0 and 57.6 kW $kg^{-1}$ is achieved, which stands for the state-of-the-art reported so far on vanadium-based electrode materials, to the best of our knowledge [6,14,20,22,30–32,34].

To further demonstrate the potential of the pseudocapacitive cathode for practical use, the rate capability of layered FeVO NSs cathodes with a high loading of 3.5 and 6.0 mg $cm^{-2}$ were further fabricated and measured. The obtained capacity is calculated based on the area current and area capacity (Fig. S9a). For a mass loading of 3.5 and 6.0 mg $cm^{-2}$, a high areal capacity of 1.20 and 2.07 mA h $cm^{-2}$ is obtained at 0.35 and 0.6 mA $cm^{-2}$, respectively. At the same area current, thick-film cathodes exhibit larger area capacity compared to that of thinner ones. The related time vs. area capacity plots (Fig. S9b) shows the fast charging and discharging ability of the thick-film cathode, such as an area capacity of ~ 0.88 mA h $cm^{-2}$ are delivered in 260 s. The tested performance of the thick-film is still not ideal since the enhanced mass loading with enlarged resistances. Further material modification or electrode re-construction is expected to improve the thick-film performance [3,36,37].

## 4. Conclusion

In this work, we demonstrate that the novel layered FeVO NSs exhibit excellent pseudocapacitive lithium storage performance. The layered FeVO NSs with ultrathin feature (less than 10 nm) are successfully synthesized by a facile wet-chemical approach with high yield. The crystalline FeVO NSs offer additional $Li^+$ storage sites in the interlayers compared to that of amorphous FeVO NPs, which delivers the enhanced capacity. The lithium storage in layered FeVO NSs cathode is a non-phase change process with only ~ 1.1% layer expansion/shrinkage. Kinetics analysis investigates over 70% of total capacity is capacitive contribution, which enables ultrahigh-rate capability. Remarkably, the FeVO NSs cathode delivers a high capacity of 350, 273 and 90 mAh $g^{-1}$ at 0.1, 1 and 20 A $g^{-1}$, respectively, and excellent cycling stability over thousands of cycles. Our work highlights the novel iron vanadate cathode that delivers the fast pseudocapacitive behavior for realizing high-rate lithium storage. We believe the next-generation asymmetric energy storage devices under the utilization of electrode materials with high pseudocapacitance will deliver remarkable performances with both high energy and high power.

## Acknowledgements

This work was supported by the National Key Research and Development Program of China (2016YFA0202603), the National Basic Research Program of China (2013CB934103), the Programme of Introducing Talents of Discipline to Universities (B17034), the National Natural Science Foundation of China (51521001), the National Natural Science Fund for Distinguished Young Scholars (51425204), the Huanghe Talents Science and Technology Program, the Fundamental Research Funds for the Central Universities (WUT: 2016III001, 2017III009), and the International Postdoctoral Exchange Fellowship Program (20160025). Prof. Liqiang Mai gratefully acknowledged financial support from China Scholarship Council (No. 201606955096).

## Appendix A. Supporting information

Supplementary data associated with this article can be found in the online version at http://dx.doi.org/10.1016/j.nanoen.2018.02.028.

## References

[1] L. Mai, X. Tian, X. Xu, L. Chang, L. Xu, Chem. Rev. 114 (2014) 11828–11862.
[2] R.C. Massé, C. Liu, Y. Li, L. Mai, G. Cao, Natl. Sci. Rev. 4 (2017) 26–53.
[3] M.R. Lukatskaya, B. Dunn, Y. Gogotsi, Nat. Commun. 7 (2016) 12647.
[4] V. Augustyn, P. Simon, B. Dunn, Energy Environ. Sci. 7 (2014) 1597–1614.
[5] Q. Wei, F. Xiong, S. Tan, L. Huang, E.H. Lan, B. Dunn, L. Mai, Adv. Mater. 29 (2017) 1602300.
[6] B.K. Lesel, J.S. Ko, B. Dunn, S.H. Tolbert, ACS Nano 10 (2016) 7572–7581.
[7] V. Augustyn, J. Come, M.A. Lowe, J.W. Kim, P.L. Taberna, S.H. Tolbert, H.D. Abruna, P. Simon, B. Dunn, Nat. Mater. 12 (2013) 518–522.
[8] T. Brezesinski, J. Wang, S.H. Tolbert, B. Dunn, Nat. Mater. 9 (2010) 146–151.
[9] P. Simon, Y. Gogotsi, B. Dunn, Science 343 (2014) 1210–1211.
[10] J.W. Kim, V. Augustyn, B. Dunn, Adv. Energy Mater. 2 (2012) 141–148.
[11] V. Augustyn, E.R. White, J. Ko, G. Grüner, B.C. Regan, B. Dunn, Mater. Horiz. 1 (2014) 219–223.
[12] J.B. Cook, H.-S. Kim, T.C. Lin, C.-H. Lai, B. Dunn, S.H. Tolbert, Adv. Energy Mater. 7 (2017) 1601283.
[13] G.A. Muller, J.B. Cook, H.-S. Kim, S.H. Tolbert, B. Dunn, Nano Lett. 15 (2015) 1911–1917.
[14] Y. Yue, H. Liang, Adv. Energy Mater. (2017) 1602545.
[15] Q. Liu, Z.F. Li, Y. Liu, H. Zhang, Y. Ren, C.J. Sun, W. Lu, Y. Zhou, L. Stanciu, E.A. Stach, J. Xie, Nat. Commun. 6 (2015) 6127.
[16] J. Wang, H. Tang, L. Zhang, H. Ren, R. Yu, Q. Jin, J. Qi, D. Mao, M. Yang, Y. Wang, Nat. Energy 1 (2016) 16050.
[17] Q. An, Q. Wei, P. Zhang, J. Sheng, K.M. Hercule, F. Lv, Q. Wang, X. Wei, L. Mai, Small 11 (2015) 2654–2660.
[18] F. Cheng, J. Chen, J. Mater. Chem. 21 (2011) 9841–9848.
[19] J.L. Durham, A.S. Poyraz, E.S. Takeuchi, A.C. Marschilok, K.J. Takeuchi, Acc. Chem. Res. 49 (2016) 1864–1872.
[20] Y. Zhao, C. Han, J. Yang, J. Su, X. Xu, S. Li, L. Xu, R. Fang, H. Jiang, X. Zou, Nano Lett. 15 (2015) 2180–2185.
[21] H. Ma, S. Zhang, W. Ji, Z. Tao, J. Chen, J. Am. Chem. Soc. 130 (2008) 5361–5367.
[22] X. Zhang, W. Yang, J. Liu, Y. Zhou, S. Feng, S. Yan, Y. Yao, G. Wang, L. Wan, C. Fang, Z. Zou, Nano Energy 22 (2016) 38–47.
[23] P. Poizot, S. Laruelle, M. Touboul, J.-.M. Tarascon, C.R. Chim, 6 2003 125–134.
[24] Q. Wei, J. Liu, W. Feng, J. Sheng, X. Tian, L. He, Q. An, L. Mai, J. Mater. Chem. A 3 (2015) 8070–8075.
[25] X. Wang, S. Kajiyama, H. Iinuma, E. Hosono, S. Oro, I. Moriguchi, M. Okubo, A. Yamada, Nat. Commun. 6 (2015) 6544.
[26] Q. Wei, Z. Jiang, S. Tan, Q. Li, L. Huang, M. Yan, L. Zhou, Q. An, L. Mai, ACS Appl. Mater. Interfaces 7 (2015) 18211–18217.
[27] Y.-N. Zhou, J. Ma, E. Hu, X. Yu, L. Gu, K.-W. Nam, L. Chen, Z. Wang, X.-Q. Yang, Nat. Commun. (2014) 5381.
[28] Z. Le, F. Liu, P. Nie, X. Li, X. Liu, Z. Bian, G. Chen, H.B. Wu, Y. Lu, ACS Nano 11 (2017) 2952–2960.
[29] J. Dong, Y. Jiang, Q. Li, Q. Wei, W. Yang, S. Tan, X. Xu, Q. An, L. Mai, J. Mater. Chem. A 5 (2017) 10827–10835.
[30] Y. Ma, A. Huang, H. Zhou, S. Ji, S. Zhang, R. Li, H. Yao, X. Cao, P. Jin, J. Mater. Chem. A 5 (2017) 6522–6531.
[31] H. Song, M. Luo, A. Wang, ACS Appl. Mater. Interfaces 9 (2017) 2875–2882.
[32] Y. Lu, J. Wu, J. Liu, M. Lei, S. Tang, P. Lu, L. Yang, H. Yang, Q. Yang, ACS Appl. Mater. Interfaces 7 (2015) 17433–17440.
[33] G. Yang, H. Song, G. Yang, M. Wu, C. Wang, Nano Energy 15 (2015) 281–292.
[34] D. Kong, X. Li, Y. Zhang, X. Hai, B. Wang, X. Qiu, Q. Song, Q.-H. Yang, L. Zhi, Energy Environ. Sci. 9 (2016) 906–911.
[35] Q. Liu, Z.-F. Li, Y. Liu, H. Zhang, Y. Ren, C.-J. Sun, W. Lu, Y. Zhou, L. Stanciu, E.A. Stach, Nat. Commun. 6 (2015) 6127.
[36] Y. Dai, Q. Li, S. Tan, Q. Wei, Y. Pan, X. Tian, K. Zhao, X. Xu, Q. An, L. Mai, Q. Zhang, Nano Energy 40 (2017) 73–81.
[37] L. Hu, F. La Mantia, H. Wu, X. Xie, J. McDonough, M. Pasta, Y. Cui, Adv. Energy Mater. 1 (2011) 1012–1017.

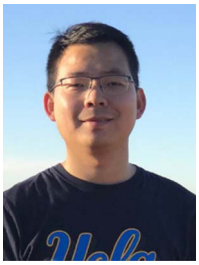

**Qiulong Wei** received his Ph.D. from the State Key Laboratory of Advanced Technology for Materials Synthesis and Processing, Wuhan University of Technology in 2016, under the supervision of Prof. Qingjie Zhang and Prof. Liqiang Mai. Currently, he is a postdoctoral fellow in the laboratory of Prof. Bruce Dunn at the Materials Science and Engineering, UCLA. His current research involves the design and synthesis of nanomaterials for achieving both high energy density and power density, electrochemical energy storage devices.

**Qinqin Wang** received her B.S. degree in Material Science and Engineering from Wuhan University of Technology in 2015. She is currently working towards the Ph.D. degree in condensed matter physics at Institute of Physics, Chinese Academy of Sciences. Her current research interests include two-dimensional materials and devices.

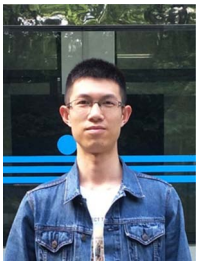

**Qidong Li** received his M.S. degree in Materials Engineering from Wuhan University of Technology in 2015. He is currently working toward the Ph.D. degree and studying as joint Ph.D. student at Argonne National Laboratory. His current research focuses on the energy storage materials and devices.

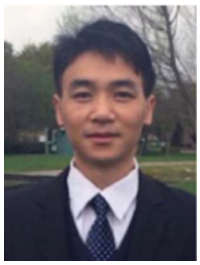

**Qinyou An** is Associate Professor of Materials Science and Engineering at Wuhan University of Technology (WUT). He received his Ph.D. degree from WUT in 2014. He carried out his postdoctoral research in the laboratory of Prof. Yan Yao at the University of Houston in 2014–2015. Currently, his research interest includes energy storage materials and devices.

**Yunlong Zhao** is a postdoctoral fellow in the Department of Chemistry and Chemical Biology at Harvard University, Cambridge, Massachusetts, USA. He received his Ph.D. degree from WUT in Material Science in 2017, under the supervision of Prof. Liqiang Mai, Prof. Qingjie Zhang and Prof. Charles Lieber. His research interests include nanoelectronics, nano-bio interface and energy storage.

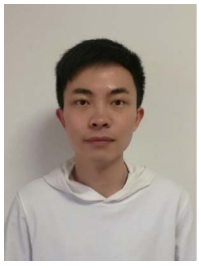

**Zhuo Peng** received his B.S. degree in Polymer Materials Science and Engineering from Hubei University in 2016. He is currently working towards the master degree in Material Science and Engineering at Wuhan University of Technology. His current research focuses on electrode materials for emerging energy storage devices.

**Yalong Jiang** received his B.S. degree in College of Material and Metallurgy from Wuhan University of Science and Technology in 2015. He is currently working toward the Ph.D. degree and focuses on energy storage materials and devices.

**Shuangshuang Tan** received his B.S. degree in Material Science and Engineering from Wuhan University of Technology in 2016. He is currently working toward the Ph.D. degree and his current research focuses on the energy storage materials and devices.

**Mengyu Yan** received his Ph.D. from the State Key Laboratory of Advanced Technology for Materials Synthesis and Processing, Wuhan University of Technology in 2016, under the supervision of Prof. Liqiang Mai. Currently, he is a research associate and WRF innovation fellow at the Materials Science and Engineering department, University of Washington. His current research involves the energy storage/conversion materials and nanoscale devices.

**Liqiang Mai** is Cheung Kong Scholar Chair Professor at Wuhan University of Technology (WUT), Distinguished Young Scholar for National Natural Science Fund of China, and Winner of National Ten Thousand Talent Plan of China. He received his Ph.D. degree from WUT in 2004 and carried out postdoctoral research in Prof. Zhonglin Wang's group at Georgia Institute of Technology (2006–2007). He worked as an advanced research scholar in Prof. Charles M. Lieber's group at Harvard University (2008–2011) and Prof. Peidong Yang's group at University of California, Berkeley (2017). His current research interests focus on nanowire materials and devices for energy storage.